Journal of
Materials Chemistry B

Accepted Manuscript

This article can be cited before page numbers have been issued, to do this please use: W. Huang, X. Wang, C. Wang, L. Du, J. Zhang, L. Deng, H. Cao and A. Dong, *J. Mater. Chem. B*, 2019, DOI: 10.1039/C8TB02706D.

ROYAL SOCIETY OF CHEMISTRY

rsc.li/materials-b

Journal Name

View Article Online
DOI: 10.1039/C8TB02706D

ARTICLE

Structural Exploration of Hydropbobic Core in Polycationic Micelles for Improving siRNA Delivery Efficiency and Cell Viability

Wenjun Huang±[a,c], , Xiaoxia Wang±[b], Changrong Wang[a], Lili Du[b], Jianhua Zhang[a], Liandong Deng[a], Huiqing Cao[b], Anjie Dong*[a,c]

Improving siRNA delivery efficiency often encounters a dilemma with poor or decreased biocompatibility for polycationic micelles. To address the dilemma, this work focused on the structural exploration of hydrophobic core in amphiphilic polycationic micelles by preparing two amphiphilic polycations with block or random hydrophobic segments, poly(ethylene glycol)-block-poly(aminoethyl methacrylate)-block-poly(2-diamylamine ethyl methacrylate)-block-poly(2-diethylamine ethyl methacrylate (mPEG-PAMA-PD5A-PDEA, PADE) and poly(ethylene glycol)-block-poly(aminoethyl methacrylate)-block-poly(2-diamylamine ethyl methacrylate-co-2-diethylamine ethyl methacrylate) (mPEG-PAMA-P(D5A/DEA), PA(D/E)). The properties of the two copolymers and their self-assembly micelles were characterized including structure, morphology, size and zeta potential. Cytotoxicity, siRNA silencing efficiency and cellular uptake of PADE/siRNA and PA(D/E)/siRNA complexes were evaluated in HepG2 and MDA-MB-231 cells in vitro. The endosome escape and intracellular distribution of PADE/siRNA and PA(D/E)/siRNA in HepG2 cells were also observed by CLSM. Significantly, the results indicated that PA(D/E)/siRNA showed not only better gene silencing efficiency but also lower cytotoxicity, which may be attributed to the homogeneous morphology of the hydrophobic core of PA(D/E) micelles. Therefore, this work provided a new pathway to overcome the dilemma between siRNA delivery efficiency and biocompatibility for development of efficient polycation carriers.

Introduction

It's worth noting that gene therapy based on small interfering RNA (siRNA) technology is a promising treatment for many kinds of diseases,[1-5] which attracts more and more attention. However, naked siRNA in vivo is easily degraded by nucleic acid enzyme, with high renal clearance rate and low endocytosis.[6,7] Hence, a key strategy of gene therapy is to select the appropriate gene carrier and gene introduction method, so that the safe, efficient, controllable and stable expression of the target gene in target cell could be obtained.[8,9] However, gene delivery has been encountered a dilemma between high transfection efficiency and good biocompatibility.

At present, the gene carriers mainly include virus vectors and non-viral vectors. Although with high transduction efficiency, viral vectors are limited for application due to immunogenicity and thus the safety concern and difficulties in preparation.[10,11] Non-viral vectors have the advantages of low toxicity and low immunogenicity,[12-15] but with the disadvantage of low transduction efficiency yet. Beside cationic liposome, various of polycationic based vectors have been prepared to delivery siRNA, such as polyethylenimine (PEI) and its derivatives,[16-19] polyamidoamine dendrimer,[20, 21] poly(L-lysine) (PLL)[22,23] and poly(2-dimethylaminoethyl methacrylate) (PDMA),[24-29] etc., because they can interact with siRNA to form nano-complexes, have structural flexibility and are easy to prepare. To balancing the biocompatibility and transduction efficiency, PEGylated (A segments) and hydrophobized (C moieties) strategies have been widely used to modify polycation (B moieties) to construct A–B–C, A–C–B, or A–(B/C) types of amphiphilic polycations for core-shell micelles,[30-37] which not only stabilized the siRNA-loaded complexes but also improved the cell uptake, resulting in high improvement in gene-silencing efficiency.

Our previous work had certificated A-B-C type of tri-block copolymer showed more promising gene delivery efficiency than A–C–B and A–(B/C).[38] Recently, we studied a series of triblock cationic copolymers, PEG block poly (aminoethyl methacrylate) (PAMA) block pH-sensitive hydrophobic segments with different pKa, and a significant discovery was obtained that the better gene silencing efficiency was located in a narrow range of pKa 5.8-6.2, which was contributed from higher endosomal escape.[39] Continuously, in this work as shown in Scheme 1, we further explored the structural contribution of the pH sensitive hydrophobic cores (pKa~6.0) with block or random monomer units of 2-(diethylamine) ethyl methacrylate (DEA) and 2-(diamylamine) ethyl methacrylate (D5A). Two kinds

a. Department of Polymer Science and Technology, School of Chemical Engineering and Technology, Key Laboratory of Systems Bioengineering (Ministry of Education), Tianjin University, Tianjin 300072, China.
b. Laboratory of Nucleic Acid Technology, Institute of Molecular Medicine, Peking University, Beijing 100871, China.
c. Collaborative Innovation Center of Chemical Science and Engineering (Tianjin), Tianjin 300072, China.
± Wenjun Huang and Xiaoxia Wang contributed equally to this work.
*Email - ajdong@tju.edu.cn

View Article Online
DOI: 10.1039/C8TB02705D

of tri-block copolymer $mPEG_{2k}$-PAMA-P (D5A/DEA) (PA(D/E)) and four-block polymer $mPEG_{2k}$-PAMA-PD5A-PDEA (PADE) were synthesized by RAFT polymerization. The molecular and micellar structures of PA(D/E) and PADE had been characterized, and the intracellular siRNA delivery capacity and cell viability had been evaluated. The results showed that the homogeneous composition and morphology of the inner core in PA(D/E) micelles facilitated both higher intracellular gene silencing efficiency and better cell viability, which will help to provide some reasonable suggestions in designing siRNA carriers.

Experimental

Materials

Methoxy PEG ($mPEG_{2k}$), azobisisobutyronitrile (AIBN), di-tert-butyl dicarbonate (Boc), 2-aminoethanol, methacryloyl chloride, 1-bromopentane, acetonitrile, dimethyl sulfoxide (DMSO), TRIzol Reagent and 3-[4,5-dimethylthiazol-2-yl]-2,5-diphenyltetrazolium bromide (MTT) were purchased from SigmaAldrich. Agarose was bought from GEN TECH (Hong Kong, China). Lipofectamine 2000, Dulbecco's modified Eagle's medium (DMEM), Opti-MEM, penicillin–streptomycin, and trypsin were purchased from Thermo Fisher. Cy5-labeled siRNA (Cy5-siRNA), siFL, and siRRM2 were supplied by Suzhou Ribo Life Science Co., Ltd. (Jiangsu, China).

Synthesis of 2-(diamyl amine) ethyl methacrylate (D5A)

Ethanolamine and 1-bromopentane were added into a three-round bottom flask with acetonitrile. In addition, Na_2CO_3 was added into reaction bottle. The reaction mixture was stirred at 80 °C for 12 h. The reaction mixture was then filtered and evaporated. The condensed product was dissolved in tetrahydrofuran and added with triethylamine. After that, methylacryloyl chloride was added slowly into the reaction bottle at 0 °C. After 12 hours of reaction, the mixed reactant was filtered and evaporated to obtain the crude product, and the product was finally obtained by vacuum distillation.

Synthesis of N-(tert-Butoxycarbonyl) aminoethyl methacrylate (A_EMA)

According to previous reports,[40] N-(tert-butoxycarbonyl) amino ethyl methacrylate was prepared. Tert-butyl N-(2-hydroxyethyl) carbamate (10 g, 62 mmol) and triethylamine (12.9 mL, 93 mmol) were added to the reaction bottle containing CH_2Cl_2 (100 mL), then methacrylate was added dropwise slowly to the mixture at 0 °C with Ar conditions. After 1 h, the reaction mixture was transferred to room temperature and continued to react for 12 h. The reaction mixture was washed with 10% citric acid, 10% HCl, 10% K_2CO_3, sat $NaHCO_3$ and brine, respectively. After that, the solution was dried by $MgSO_4$ and removed the solvent under reduced pressure. Finally, the desired product was purified by recrystallization using a mixture of dichloromethane and n-hexane (v/v = 1/9).

Synthesis of $mPEG_{2k}$-b-PA_EMA(PA_E)

The polymer of $mPEG_{2k}$-b-PA_EMA was synthesized by a reversible addition-fragmentation chain transfer (RAFT) polymerization of A_EMA monomers using AIBN as the initiator. Firstly, the RAFT agent was prepared and subsequently the mPEG-based macro-RAFT agent ($mPEG_{2k}$-DDMAT) was synthesized by esterification reaction of $mPEG_{2k}$ and S-dodecyl-S'-(□,□'-dimethyl- ''-acetic acid)-trithiocarbonate (DDMAT).[41,42] Typically, AIBN, $mPEG_{2k}$-DDMAT and AEMA were added into the Schlenk tube with 2 mL of dimethylformamide (DMF). The polymerization reaction was achieved at 70 °C for 24 h, then the mixture was dialyzed for 48 h in double distilled water and freeze-dried to get the polymer.

Synthesis of $mPEG_{2k}$-b-PA_EMA-b-PD5A-b-PDEA (PA_EDE) and $mPEG_{2k}$-b-PA_EMA-b-P(D5A/DEA) (PA_ED/E)

The tri-block polymer PA_EDE and four-block polymer PA_E(D/E) were synthesized by a method of RAFT polymerization as shown in Fig. 1. The former adopted the method of adding monomers in a certain order, the latter took a method of adding two monomers together. Briefly, the polymerization reaction was achieved at 70 °C for 24 h. Then the mixture was dialyzed for 48 h in double distilled water and freeze-dried to get the copolymers.

Synthesis of $mPEG_{2k}$-PAMA-PD5A-PDEA (PADE) and $mPEG_{2k}$-PAMA-P(D5A/DEA) (PA(D/E))

Trifluoroacetic acid (TFA) was used as a deprotection agent to deprotect the boc-protection on PA_EDE and PA_E(D/E). Then the deprotected copolymers were dialyzed for 48 hours in double distilled water and freeze-dried to get the copolymers PADE and PA(D/E). The copolymers were characterized using ^1H NMR. (Varian Unity Plus INOVA 400).

Preparation and characterization of PADE and PA(D/E) micelles

10 mg PADE or PA(D/E) were dissolved in 1 mL trifluoroethanol (TFE) and the obtained solution was added dropwise slowly into 5 mL double-distilled water under stirring. Then the solution was dialyzed against deionized water for two days, completely removing TFE and obtaining PADE or PA(D/E) micelles. The dynamic laser scattering (Zetasizer Nano ZS, Malvern, UK) was used to measure the size distribution and zeta potential of the micelles. In addition, transmission electron microscopy (TEM, JEM-100CX, Philips EM400ST) was used to observe the morphologies of the micelles.

Measurements of pKa values

The acid-base titration method[43] was performed to test the pKa values of PADE and PA(D/E). Briefly, the copolymer was first dissolved in HCl (0.1 M), and then added 50 □L NaOH (0.1 M) each time under vigorous stirring. The Mettler Toledo pH meter with microelectrode was used to detect the pH changes. pKa was defined as the pH value between the two equivalent points in the titration curve.

Differential Scanning Calorimeter (DSC) measurements

The DSC measurements were performed by using the Netzsch DSC 200 F3 under a constant flow of nitrogen of 50 mL/min. The freeze-dried powder of PADE or PA(D/E) micelles were used to explore the crystallization of PADE or PA(D/E) micelles. 10 mg sample was added into a Tzero aluminum hermetic DSC pan. The sample pan was placed into the DSC well, which was cooled to 0 °C in advance. In the experiment, the DSC curve was recorded from 0 °C to 300 °C at a rate of 5 °C/min.

The pH-sensitivity assembly/disassembly behavior.

The pH-sensitivity of polymer micelles was evaluated by Nile red based fluorescent probe method. In brief, the 20 g of Nile red dye was encapsulated into PADE or PA(D/E) micelles (1 mg/mL) by hydrophobic interaction, which was used to measure the micellar assembly/disassembly states by track the fluorescent signal of Nile red dye. The pH of the Nile red loaded micelle solution was subsequently regulated to 7.4, 7.2, 7.0, 6.8, 6.5, 6.2, 6.0, 5.8, 5.6, 5.2, 4.5, 4.0, 3.5, 3.0 and 2.4. After 2 h, the Varian fluorescence spectrophotometer (Varian, USA) was used to measure the fluorescent value of the micelles solution.

Preparation of siRNA-loaded complexes

The PADE or PA(D/E) micelles/siRNA complex was prepared by electrostatic self-assembly. The copolymer micelle dispersion was mixed with the same volume of siRNA solution, and repeatedly blow several times or high speed concussion 5 s, and then incubate for 20 min at room temperature for using.

Agarose gel electrophoresis assay

The agarose gel retardation assay was carried out as follows: 20 μL copolymer micelles (CMs)/siRNA complex solution (N/P = 2, 5, 8, 10) was fully mixed with 4 μL of 6 x loading buffer (Takara Biotechnology, Dalian, Liaoning Province, China), the mixture was then totally loaded onto 2% agarose gel containing 5 μg/mL ethidium bromide. Electrophoresis was carried out for 30 min at 120 V voltage when the electrophoresis buffer reached 1 × TAE. At last, the results of the siRNA electrophoresis were viewed at UV light wavelength of 254 nm with an image master VDS thermal imaging system (Bio-Rad, Hercules, CA).

In vitro gene silencing

To evaluate the gene silencing ability of copolymer micelles/siFL, the MDA-MB-231-Luc cells and HepG2-Luc cells were plated in 24-well plates with 5×10^4 cells each well for 24 h. Subsequently, the medium was removed and added Opti-MEM (600 μL) containing 0.4 g copolymer micelles/siFL (N/P =5, 10, 15). After 24 h incubation, the culture medium was removed and the cells were washed with PBS for three times. Then, the cells were lysed using 100 μL of 1 × passive lysis buffer (Promega Co., Madison, WI) for 30 min and accompanied by violent shaking to ensure complete lysis. After that, the cell lysate was centrifuged and the fluorometer (Synergy HT, BioTek, USA) was used to measure the relative luminescence intensity.

The reverse transcription polymerase chain reaction (RT-PCR) assay was performed to evaluate the gene-silencing efficiency of mRNA level. Briefly, the HepG2 cells were plated in 6-well plates (2×10^5 cells each well) for 24 h, the PADE/siRRM2 and PA(D/E)/siRRM2 complexes were used to transfect cells and then incubated for 24 h. The total RNA was extracted using a TRIzol Reagent (Thermo Fisher) and converted to cDNA by reverse transcription. Then, the RT-PCR assay was performed by using a SYBR Green PCR Master Mix with GAPDH as the internal control.

Cell viability

MTT assay was carried out to evaluate the cytotoxicity of PADE/siRNA and PA(D/E)/siRNA complexes. After the HepG2 cells or were seeded in 96-well plates (1×10^4 cells per well) for 24 h, the siRNA-loaded copolymer micelles (N/P = 5, 10, and 15; siNC dose: 30 nM, 50 nM) were used to treat the cells for 24 h, after incubation for 24 h, 10 μL of MTT solution with a concentration of 5 mg/mL in PBS was added in each well and incubated for 4 h. Then, the medium was replaced with DMSO (50 μL/well) to dissolve the formazan crystals. The Multi-Mode Microplate Reader was used to measure the absorbance at 540 nm (650 nm used as the reference wavelength). The untreated cells were used as controls.

In virto cellular uptake and cellular distribution

The HepG2 cells and MDA-MB-231 cells were used. The cells plated in 6-well plates (2×10^5 cells each well) for 24 h before transfection for cellular uptake studies. After 24 h incubation, the Cy5-siRNA-loaded copolymer micelles (N/P = 5, 10; Cy5-siRNA: 30 nM, 50 nM) were used to treat the cells for 4 h at 37 °C. Then, remove the culture medium and wash it three times with 1 mL PBS to remove the residual free complexes, and followed by suspended in PBS. The fluorescence signal was then detected by a FACS Calibur flow cytometer (Becton Dickinson, San Jose, CA, USA).

The cells were seeded in 35 mm dishes with 2×10^5 cells each well for 24 h to evaluate the cellular distribution. After 24 h, the cells were treated with the PADE/Cy5-siRNA and PA(D/E)/Cy5-siRNA (N/P = 5, 10, and 15; siRNA dose: 30 nM, 50 nM) and incubated for 4 h. After incubation, remove the liquid and wash with cold PBS for 3 times. Subsequently, DAPI was used to mark cell nuclei and Lysotracker Green was used to mark endosome/lysosome. After the staining, the cells were washed with PBS for 3 times, and Zeiss confocal microscope (LSM700, Carl Zeiss, Germany) was used to observe the fluorescence and take photos.

Results and discussion

Preparation and characterization of PADE and PA(D/E)

Firstly, the monomer 2-(diamyl amine) ethyl methacrylate (D5A-MA) was prepared. The four-block copolymers PADE was prepared by sequential RAFT of N-(tert-butoxycarbonyl) aminoethyl methacrylate (A_EMA), 2-(diethylamine) ethyl methacrylate (D5A), and 2-(diamyl amine) ethyl methacrylate (DEA) monomers. Difference from the four-block polymer, PA(D/E) was prepared by adding the mixture of two monomers

in the second step of RAFT polymerization (Fig. 1). The structures of D5A-MA and the intermediate products PA_E, PA_ED, PA_EDE, $PA_E(D/E)$ were confirmed by the proton NMR (^{1}H NMR) spectra (Fig. 2A). The disappearance of the peaks at b3 and b5 (Fig. 2B and 2C) confirmed PADE and PA(D/E) were synthesized successfully. The degree of polymerization of each component of the two polymers was calculated by ^{1}H NMR, labeled as $mPEG_{45}$-$PAMA_{30}$-$PD5A_{31}$-$PDEA_{36}$ (PADE) and $mPEG_{45}$-$PAMA_{30}$-$P[D5A_{29}/DEA_{29}]$ (PA(D/E)). Then the molecular weight could be calculated as shown in Table 1. In addition, the gel permeation chromatography was used to measure the polydispersity index of PADE and PA(D/E) copolymers, as listed in Table1.

Characterization of PADE and PA(D/E) micelles

As amphiphilic copolymers, PADE and PA(D/E) could self-assemble into micelles, which could bind siRNA by electrostatic interactions. Dynamic light scattering (DLS) and transmission electron microscopy (TEM) were used to determine the size distribution and morphology of PADE and PA(D/E) micelles, respectively. As showed in Fig. 3, PADE and PA(D/E) micelles all possessed spherical structures with similar size about 90 nm and narrow particle size distributions. The acid-base titration curves (Fig. 4A) certificated that PADE and PA(D/E) had similar pKa□6.0, but PADE showed two transitions at pH 4.0 and 6.8, supposing to be leaded by the block structure of PD5A and PDEA segments. Hydrophobic Nile red dye was used as the fluorescent probe encapsulated into the micellar hydrophobic core to track the pH sensitive assembly/disassembly behavior. As shown in Fig. 4B and 4C, the fluorescent signal of Nile red dye weakened gradually with pH decreasing and became undetectable, indicating the hydrophobic environment of the core gradually disappeared due to micellar disassembly with the protonation of DEA and D5A moieties in the core. Also, different from PA(D/E) micelles with a continuous variation in fluorescent signal, PA(D/E) micelles showed two steps of decrease, indicting two phases maybe exist in PA(D/E) micellar cores. The further evaluation results of PADE and PA(D/E) micelles by DSC were shown in Fig. 4D. The DSC curve of PADE exhibited two melting peaks at 150 °C and 225 °C, assigned to the PD5A and PDEA crystalline phases, respectively. For PA(D/E), only one melting peak at about 215 °C was observed. Therefore, it could be thought the hydrophobic core of PA(D/E) micelle took a homogeneous morphology and that of PADE micelle took microphase separation structure as shown in Scheme 1. Besides, PA(D/E) micelles showed slightly higher zeta potential (34 mV) than that of PADE (29 mV) (Fig. 4E), while they possessed similar siRNA bonding capacity completely at a N/P ratio of 5.0 (Fig. 4F).

About the difference of zeta potential between PA(D/E) and PADE, we speculated that the structure difference of hydrophobic cores between PA(D/E) and PADE micelles may attribute to the difference in zeta potential. To certificate this speculation, we synthesized two kinds of copolymers without the cationic block by RAFT polymerization, poly(ethylene glycol)-block-poly(2-diamylamine ethyl methacrylate)-block-poly(2-diethylamine ethyl methacrylate (mPEG-PD5A-PDEA, PDE) and poly(ethylene glycol)-block-poly(2-diamylamine ethyl methacrylate-co-2-diethylamine ethyl methacrylate) (mPEG-P(D5A/DEA), P(D/E)). The ^{1}H NMR spectra were taken to characterize the structure of PDE and P(D/E), and the zeta potentials of PDE and P(D/E) micelles were evaluated(shown in Fig. S1A and B). P(D/E) micelles with slightly higher zeta potential(16mV) than that of PDE(12mV). The pKa values of DEA and D5A are about 8.5 and 5.0, respectively, which means DEA moieties are facile to be charged positively in the testing medium of double-distilled water (pH»7.0). The higher zeta potential of P(D/E) micelles indicated that there are more positive charged DEA moieties on the core-shell interface of P(D/E) micelles due to the random core structure than that of PDE micelles with block core structure. Therefore, it could be thought that the higher zeta potential of the random structural core(D/E) lead to the higher zeta potential of PA(D/E).

In vitro gene silencing efficiency and internalization

The luciferase assay was performed to estimate the capacity of PADE and PA(D/E) micelles in siRNA delivery in the MDA-MB-231-Luc cells and HepG2-Luc cells. As shown in Fig. 5A, in MDA-MB-231-Luc cells, PA(D/E)/siRNA complex showed higher gene silencing efficiency at 24 h than PADE/siRNA complex at the same N/P ratios and it was worth noticing that all the gene silencing efficiencies of PA(D/E)/siRNA complex at N/P = 5, 10, 15 were higher than lipo 2000. Importantly, PA(D/E)/siRNA complex could maintain the more dominance in gene silencing efficiency after 48 hours (Fig. 5B). In HepG2-Luc cells, as shown in Fig. 5C and 5D, PA(D/E)/siRNA and PADE/siRNA showed the similar luciferase silencing effects at 24 h or 48 h, which were also better than Lipo 2000 at N/P = 15. In addition, it could be seen that PA(D/E)/siRNA presented higher gene silencing efficiency in MDA-MB-231-Luc cells than HepG2-Luc cells.

To further confirm the gene delivery capacities of PA(D/E)/siRNA and PADE/siRNA, RT-PCR assay were carried out by using siRRM2. Ribonucleotide reductase M2 (RRM2) has great significance for DNA synthesis and cell growth control, which has made it an important target for cancer treatment.[44] As shown in Fig. 6A and B, both at 30nm and 50 nm doses of siRNA, PA(D/E)/siRRM2 obtained higher knockdown efficiencies in the RRM2 mRNA expression than PADE/siRRM2 at N/P = 10 and N/P = 15, which reached the level of Lipo 2000.

After 4 h incubation, fluorescence-activated cell sorting (FACS) was performed to evaluate the percentage of the cells that internalized Cy5-siRNA-loaded micelles (N/P = 5, 10) (Fig. 6 C,D,E,F). The results of mean fluorescence intensity in HepG2 cells (Fig. 6 C,D) clearly indicated that Cy5-siRNA-loaded PADE and PA(D/E) micelles showed similar cell uptake efficiencies at N/P = 5, however, the PA(D/E) showed a higher uptake efficiency than PADE at N/P = 10. In MDA-MB-231 cells (Fig. 6 E,F), obviously higher cell uptake levels of PA(D/E)/siRNA than PADE/siRNA were observed at different N/P ratios. The higher cell uptake of PA(D/E)/siRNA was related to high zeta potentials of PA(D/E) than PADE micelles as shown in Fig. 4A, resulting in higher gene silence efficiency of PA(D/E)/siRNA. Moreover, from the cell uptake results in Fig. 6(C,D,E,F), with Lipo 2000 as control, it could be seen that both PA(D/E)/siRNA and PADE

View Article Online
DOI: 10.1039/C8TB02706D

/siRNA showed obviously higher cell uptake levels in MDA-MB-231 cells than HepG2 cells, and more higher level of cell uptake for PA(D/E)/siRNA than PADE /siRNA showed in MDA-MB-231 cells. Therefore, the higher cell uptake of PA(D/E)/siRNA resulted in higher gene silence efficiency in MDA-MB-231 cells than in HepG2 cells. Noticeably, PA(D/E)/siRNA presented very low cell uptake compared with Lipo2000, but higher or similar gene silence were obtained, which was attributed the higher intracellular endosome escape efficiency than Lipo2000 due to suit pKa□6.0 certificated in our previous work.[29, 39]

Intracellular distribution of siRNA-Loaded Micelles

The important way to improve the efficiency of gene silencing efficiency is to achieve the successful escape of siRNA vector from the endosome. Confocal laser scanning microscopy (CLSM) was performed to evaluate the escape capacity and the intracellular distribution of PADE and PA(D/E)/siRNA complexes at different N/P ratio. The localization of PADE and PA(D/E)/siRNA complexes were identified by Cy5 dye labeled siRNA, Lysotracker Green labeled endosome and DAPI marked cell nuclei, as shown in Fig. 7A and 7B. The results of the colocalization ratio of red signals (Cy5-siRNA) in endosomes were showed in Fig. 7C. Increase of N/P ratios could enhance the endosomal escape of PADE and PA(D/E)/siRNA complexes, but the different core morphologies nearly lead to no effect on the endosomal escape, maybe due to the similar pKa. Our previous study on PEG blocked PAMA series of amphiphilic copolymer micelles with different pKa indicated that a narrow range of pKa 5.8-6.2 facilitated endosomal escape and leaded to significant enhancement in gene silencing efficiency.[39] Therefore, the higher gene silencing efficiency of PA(D/E)/siRNA than PADE/siRNA was supposed as to the higher internalization. It could be seen from Fig. 7C, even with the suitable pKa, the endosomal escape ability of PA(D/E)/siRNA and PADE/siRNA remained large space to be improved. Definitely, further works need to be done to explore a more reasonable micellar structure to enhance the endosomal escape.

In vitro cytotoxicity

The MTT assay was used to evaluate the in vitro cytotoxicity of PADE and PA(D/E) toward HepG2 cells, and the viability of cells at 24 h and 48 h were shown in Fig. 8. The increase of siRNA dose reduced the biocompatibility of siRNA-loaded micelles and the cytotoxicity of the two copolymer micelles/siRNA was positively correlated with N/P ratio, owing to the higher charge density could lead to more damage in cell membrane.[45] Significantly, the cell viability of PA(D/E)/siRNA was superior to PADE/siRNA at various N/P ratios, especially at higher N/P ratio (N/P= 15) and higher siRNA dose (50nM). Noticeably, the cells treated with PA(D/E/siRNA (N/P = 5, 10) at 48 hours still kept high level of viability (Fig. 8C and D).

The dilemma between the higher gene silencing efficiency and lower biocompatibility keeps egging the design of polycation micelles as gene vectors. In this work, we obtained the encouraging results that PA(D/E) with higher positive zeta potential showed not only better gene silencing efficiency but also lower cytotoxicity than PADE. We thought the advantage properties of PA(D/E) micelles may be attributed to the homogeneous morphology of the hydrophobic core. The hemolysis percentage and cell viability of PADE, PA(D/E), PDE, and P(D/E) micelles were tested and shown in Fig.S2A and B, respectively. It was observed PADE micelles showed higher hemolysis and lower cell viability than PA(D/E) micelles, and similarly, PDE showed slightly higher hemolysis and lower cell viability than P(D/E) in spite of the P(D/E) with higher positive zeta potential than PDE(Fig.S1B). Beside the possitive charges, hydrophobic interaction is an important factor to disturb cell membrane and thus increasing hemolysis and cell toxicity. As discussion above, the lower zeta potential of PDE micelles than P(D/E) indicated more D5A moieties with longer hydrophobic alkyl groups tended to distribute on the core-shell interface of PDE micelles and led to stronger hydrophobic interaction of PDE micelles with cell membrane. For P(D/E) micelles, the random structure of D5A and DEA moieties limited the interface distribution of D5A moieties, resulting in weaker hydrophobic interaction bwtween P(D/E) micelles and cells. The effect on hemolysis and cell toxicity induced by the hydrophobic interaction outweighed the effect led by slight difference in zeta potential, so P(D/E) micelles showed higher cell viability although higher positive zeta potential than PDE micelles. By the same reason, PA(D/E) showed higher cell viability than PADE in spite of higher positive zeta potential of the PA(D/E) than PADE.

Together with the higher cell uptake and siRNA delivery efficiency, the better cell viability certificated PA(D/E) micelles could be a kind of potentially biocompatible carrier for siRNA delivery. At the same time, these results suggested the dilemma between the higher gene silencing efficiency and lower biocompatibility for polycationic micelles could be resolved by the rational structure design of the micelles. Actually, based on this work, further research works are needed to deeperly disclose the reasonable polycation structure for balancing the gene silencing efficiency and biocompatibility.

Conclusions

In this paper, morphology contribution of the pH-sensitive hydrophobic core in amphiphipic polycationic micelles to the siRNA delivery efficiency and biocompatibility was discussed. Two kinds of amphiphipic poly(aminoethyl methacrylate) (PAMA) based polycations with different monomer unit sequences of 2-(diethylamine) ethyl methacrylate (DEA) and 2-(diamylamine) ethyl methacrylate (D5A) were prepared, i.e. four-block copolymer $mPEG_{2k}$-PAMA-PD5A-PDEA (PADE) and tri-block copolymer $mPEG_{2k}$-PAMA-P(D5A/DEA) (PA(D/E)). The PA(D/E) micelle with a homogeneous core due to random distribution of D5A and DEA units showed higher positive zeta potential than PADE micelle with a microphase separation structure. The results obtained from *in vitro* luciferase assay, MTT assay and RT-PCR assay indicated that PA(D/E)/siRNA showed both better cell viability and higher luciferase silencing efficiency and RRM2 gene knockdown efficiency than PADE/siRNA. The higher gene silencing efficiency of

PA(D/E)/siRNA was attributed the higher cell uptake, which indicated higher cell uptake may not result in higher cytotoxicity. Therefore, the homogenous core structure together with suit pKa could enhance gene silencing efficiency and biocompatibility at the same time. That is to say, the dilemma between the higher gene silencing efficiency and lower biocompatibility that has troubled polycationic micelles as gene vectors could be resolved by the rational structure design of the micellar core.

Conflicts of interest

There are no conflicts to declare.

Acknowledgements

This work was supported by grants from the National Natural Science Foundation of China (No. 31671021, 81502586, and 81773622).

Notes and references

1 D. Bumcrot, M. Manoharan, V. Koteliansky and D. W. Sah, *Nat. Chem. Biol.*, 2006, **2**, 711-719.
2 S. M. Elbashir, J. Harborth, W. Lendeckel, A. Yalcin, K. Weber and T. Tuschl, *Nature*, 2001.
3 S. M. Hammond, E. Bernstein, D. Beach and G. J. Hannon, *Nature*, 2000, **404**, 293.
4 G. J. Hannon, *Nature*, 2002, **418**, 244.
5 K. V. Morris, S. W. Chan, S. E. Jacobsen and D. J. Looney, *Science*, 2004, **305**, 1289-1292.
6 S. C. Semple, A. Akinc, J. Chen, A. P. Sandhu, B. L. Mui, C. K. Cho, D. W. Sah, D. Stebbing, E. J. Crosley, E. Yaworski, I. M. Hafez, J. R. Dorkin, J. Qin, K. Lam, K. G. Rajeev, K. F. Wong, L. B. Jeffs, L. Nechev, M. L. Eisenhardt, M. Jayaraman, M. Kazem, M. A. Maier, M. Srinivasulu, M. J. Weinstein, Q. Chen, R. Alvarez, S. A. Barros, S. De, S. K. Klimuk, T. Borland, V. Kosovrasti, W. L. Cantley, Y. K. Tam, M. Manoharan, M. A. Ciufolini, M. A. Tracy, A. de Fougerolles, I. MacLachlan, P. R. Cullis, T. D. Madden and M. J. Hope, *Nat. Biotechnol.*, 2010, **28**, 172-176.
7 N. P. Truong, W. Gu, I. Prasadam, Z. Jia, R. Crawford, Y. Xiao and M. J. Monteiro, *Nat. Commun.*, 2013, **4**, 1902.
8 E. Keles, Y. Song, D. Du, W. J. Dong and Y. Lin, *Biomater. Sci.*, 2016, **4**, 1291-1309.
9 Y. Yue and C. Wu, *Biomater. Sci.*, 2013, **1**, 152-170.
10 J. Kota, R. R. Chivukula, K. A. O'Donnell, E. A. Wentzel, C. L. Montgomery, H. W. Hwang, T. C. Chang, P. Vivekanandan, M. Torbenson and K. R. Clark, *Cell*, 2009, **137**, 1005-1017.
11 L. Yin, Z. Song, K. H. Kim, N. Zheng, N. P. Gabrielson and J. Cheng, *Adv. Mater.*, 2013, **25**, 3063-3070.
12 X. Bai, M. Kong, X. Wu, C. Feng, H. Park and X. Chen, *J. Mater. Chem. B.*, 2018, **6**, 5910-5921.
13 M. Khan, Z. Y. Ong, N. Wiradharma, A. B. Attia and Y. Y. Yang, *Adv. Healthc. Mater.*, 2012, **1**, 373-392.
14 V. Leiro, J. P. Garcia, P. M. D. Moreno, A. P. Spencer, M. Fernandez-Villamarin, R. Riguera, E. Fernandez-Megia and A. Paula Pêgo, *J. Mater. Chem. B.*, 2017, **5**, 4901-4917.
15 E. Mastrobattista and W. E. Hennink, *Nat. Mater.*, 2011, **11**, 10-12.
16 T. Bus, C. Englert, M. Reifarth, P. Borchers, M. Hartlieb, A. Vollrath, S. Hoeppener, A. Traeger and U. S. Schubert, *J. Mater. Chem. B.*, 2017, **5**, 1258-1274.
17 M. Gunther, J. Lipka, A. Malek, D. Gutsch, W. Kreyling and A. Aigner, *Eur. J. Pharm. Biopharm.*, 2011, **77**, 438-449.
18 L. Kong, J. Qiu, W. Sun, J. Yang, M. Shen, L. Wang and X. Shi, *Biomater. Sci.*, 2017, **5**, 258-266.
19 D. Zhu, H. Yan, Z. Zhou, J. Tang, X. Liu, R. Hartmann, W. J. Parak, N. Feliu and Y. Shen, *Biomater. Sci.*, 2018, **6**, 1800-1817.
20 X. Liu, C. Liu, E. Laurini, P. Posocco, S. Pricl, F. Qu, P. Rocchi and L. Peng, *Mol. Pharm.*, 2012, **9**, 470-481.
21 T. Yu, X. Liu, A. L. Bolcato-Bellemin, Y. Wang, C. Liu, P. Erbacher, F. Qu, P. Rocchi, J. P. Behr and L. Peng, *Angew. Chem. Int. Ed. Engl.*, 2012, **51**, 8478-8484.
22 M. Byrne, D. Victory, A. Hibbitts, M. Lanigan, A. Heise and S.-A. Cryan, *Biomater. Sci.*, 2013, **1**, 1223.
23 A. Kano, K. Moriyama, T. Yamano, I. Nakamura, N. Shimada and A. Maruyama, *J. Control. Release.*, 2011, **149**, 2-7.
24 C. Zhu, S. Jung, S. Luo, F. Meng, X. Zhu, T. G. Park and Z. Zhong, *Biomaterials*, 2010, **31**, 2408-2416.
25 S. Guo, Y. Huang, W. Zhang, W. Wang, T. Wei, D. Lin, J. Xing, L. Deng, Q. Du, Z. Liang, X. J. Liang and A. Dong, *Biomaterials*, 2011, **32**, 4283-4292.
26 Y. Huang, D. Lin, Q. Jiang, W. Zhang, S. Guo, P. Xiao, S. Zheng, X. Wang, H. Chen, H. Y. Zhang, L. Deng, J. Xing, Q. Du, A. Dong and Z. Liang, *Biomaterials*, 2012, **33**, 4653-4664.
27 S. Guo, Y. Qiao, W. Wang, H. He, L. Deng, J. Xing, J. Xu, X.-J. Liang and A. Dong, *J. Mater. Chem.*, 2010, **20**, 6935.
28 D. Lin, Y. Huang, Q. Jiang, W. Zhang, X. Yue, S. Guo, P. Xiao, Q. Du, J. Xing, L. Deng, Z. Liang and A. Dong, *Biomaterials*, 2011, **32**, 8730-8742.
29 J. Zhou, Y. Wu, C. Wang, Q. Cheng, S. Han, X. Wang, J. Zhang, L. Deng, D. Zhao, L. Du, H. Cao, Z. Liang, Y. Huang and A. Dong, *Nano. Lett.*, 2016, **16**, 6916-6923.
30 W. Chen, Y. Yuan, D. Cheng, J. Chen, L. Wang and X. Shuai, *Small*, 2014, **10**, 2678-2687.
31 T. K. Endres, M. Beck-Broichsitter, O. Samsonova, T. Renette and T. H. Kissel, *Biomaterials*, 2011, **32**, 7721-7731.
32 H. J. Kim, K. Miyata, T. Nomoto, M. Zheng, A. Kim, X. Liu, H. Cabral, R. J. Christie, N. Nishiyama and K. Kataoka, *Biomaterials*, 2014, **35**, 4548-4556.
33 J. Qian and C. Berkland, Polym. Chem., 2015, 6, 3472-3479.
34 T. M. Sun, J. Z. Du, L. F. Yan, H. Q. Mao and J. Wang, *Biomaterials*, 2008, **29**, 4348-4355.
35 T. M. Sun, J. Z. Du, Y. D. Yao, C. Q. Mao, S. Dou, S. Y. Huang, P. Z. Zhang, K. W. Leong, E. W. Song and J. Wang, *ACS Nano*, 2011, **5**, 1483.
36 X. Xu, J. Wu, Y. Liu, P. E. Saw, W. Tao, M. Yu, H. Zope, M. Si, A. Victorious, J. Rasmussen, D. Ayyash, O. C. Farokhzad and J. Shi, *ACS Nano*, 2017, **11**, 2618-2627.
37 X. Xu, J. Wu, Y. Liu, M. Yu, L. Zhao, X. Zhu, S. Bhasin, Q. Li, E. Ha, J. Shi and O. C. Farokhzad, *Angew. Chem. Int. Ed. Engl.*, 2016, **55**, 7091-7094.
38 C. Wang, L. Du, J. Zhou, L. Meng, Q. Cheng, C. Wang, X. Wang, D. Zhao, Y. Huang, S. Zheng, H. Cao, J. Zhang, L. Deng, Z. Liang and A. Dong, *ACS Appl. Mater. Interfaces.*, 2017, **9**, 32463-32474.
39 L. Du, C. Wang, L. Meng, Q. Cheng, J. Zhou, X. Wang, D. Zhao, J. Zhang, L. Deng, Z. Liang, A. Dong and H. Cao, *Biomaterials*, 2018, **176**, 84-93.
40 K. Kuroda and W. F. Degrado, *J. Am. Chem. Soc.*, 2005, **127**, 4128-4129.
41 J. Chiefari, Y. K. Chong, F. Ercole, J. Krstina, J. Jeffery, T. P. T. Le, R. T. A. Mayadunne, G. F. Meijs, C. L. Moad and G. Moad, *Macromolecules*, 1999, **31**, 5559-5562.
42 J. T. Lai, A. Debby Filla and R. Shea, *Macromolecules*, 2002, **35**, 6754-6756.
43 K. Zhou, Y. Wang, X. Huang, K. Luby-Phelps, B. D. Sumer and J. Gao, *Angew. Chem. Int. Ed. Engl.*, 2011, **50**, 6109-6114.
44 J. Shao, B. Zhou, B. Chu and Y. Yen, *Current. Cancer. Drug. Targets.*, 2006, **6**, 409.

45 L. Peng, Y. Gao, Y. N. Xue, S. W. Huang and R. X. Zhuo, *Biomaterials*, 2010, **31**, 4467-4476.

View Article Online
DOI: 10.1039/C8TB02706D

View Article Online
DOI: 10.1039/C8TB02706D

Table 1. The molecular structure, molecular weight and PDI of PADE and PA(D/E)

Polymer name	molecular structure[a]	*Mn*[b] (10^4 g/mol)	PDI[c]	pKa
PADE	$mPEG_{45}$-$PAMA_{30}$-$PD5A_{31}$-$PDEA_{36}$	2.09	3.14	6.0
PA(D/E)	$mPEG_{45}$-$PAMA_{30}$-$P(D5A_{29}$-co-$DEA_{29})$	1.90	3.22	6.0

[a]The molecular structure of the polymer was determined by ^{1}H NMR.
[b]The mean molecular weight (*Mn*) of copolymers was estimated by ^{1}H NMR.
[c]PDI=*Mw*/*Mn* measured by GPC.

View Article Online
DOI: 10.1039/C8TB02706D

Figure Captions

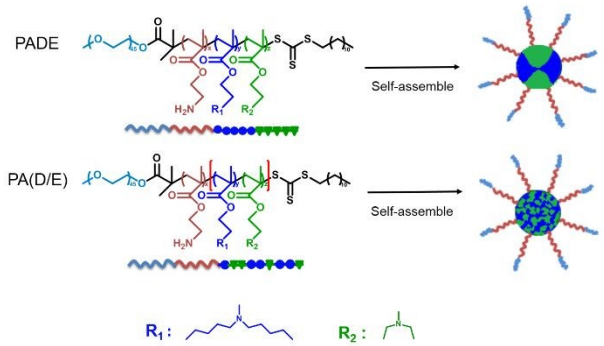

Scheme 1. Molecular Structures of PADE and PA(D/E) and their self-assemble micelles.

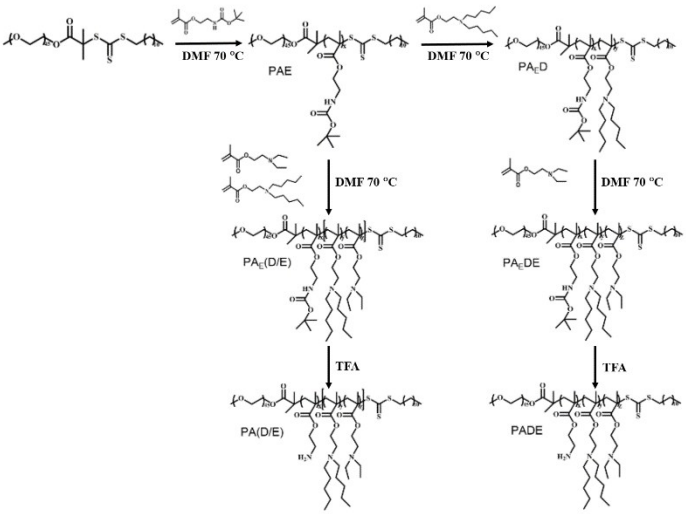

Fig. 1. Synthesis routes of copolymers PADE and PA(D/E).

View Article Online
DOI: 10.1039/C8TB02706D

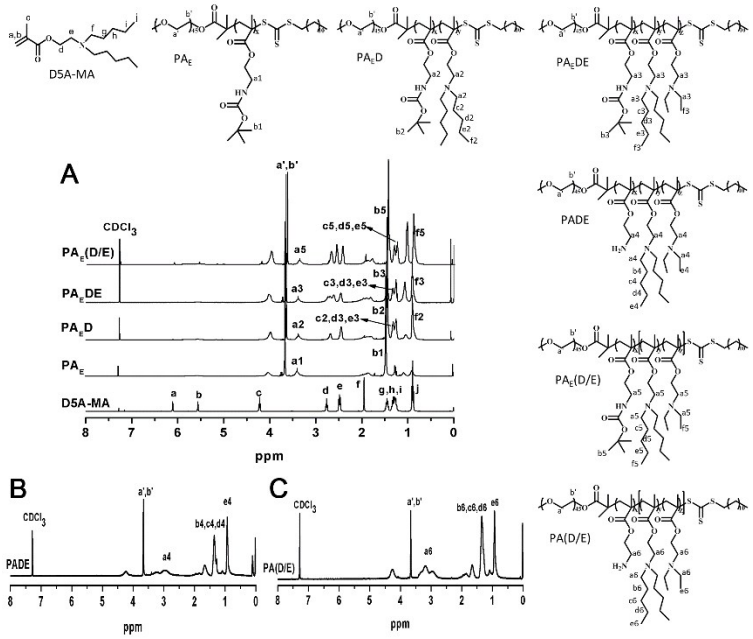

Fig. 2. ^{1}H NMR spectra of D5A-MA, PAE, PAED, PAEDE, PAE(D/E), PADE and PA(D/E).

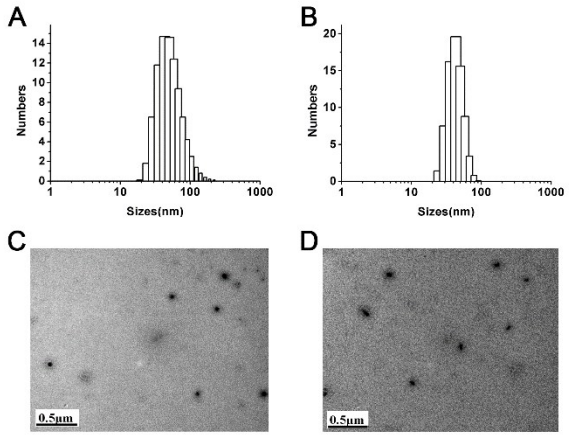

Fig. 3. Characterization of two copolymers: size distribution and TEM images of PADE (A, C), size distribution and TEM images of PA(D/E) (B, D).

View Article Online
DOI: 10.1039/C8TB02706D

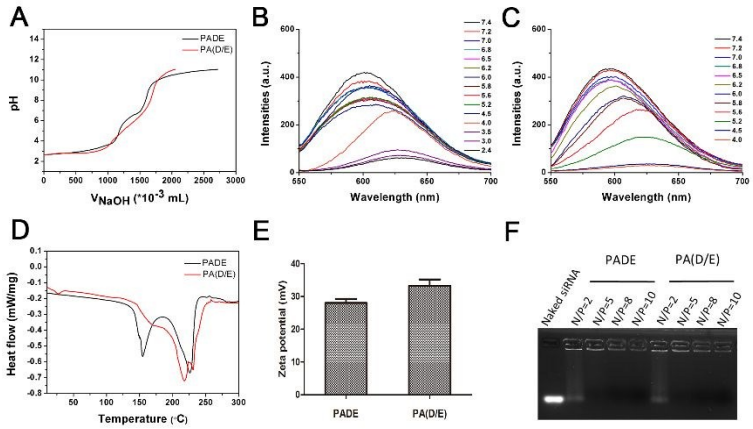

Fig. 4. (A) The pKa of PADE and PA(D/E). (B) The pH sensitive assembly/disassembly behavior of PADE. (C) The pH sensitive assembly/disassembly behavior of PA(D/E). (D)DSC thermograms of PADE and PA(D/E). (E) Zeta potential values of two copolymers micelles measured by DLS. (F) Agarose gel retardation assay of siRNA-loaded micelles.

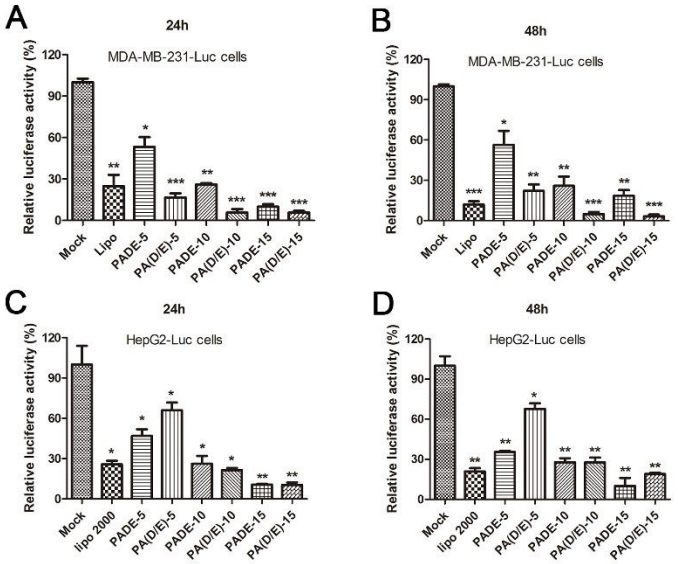

Fig. 5. In vitro luciferase expression silencing of PADE and PA(D/E) /siRNA complexes with the transfection concentrations of siRNA (siRNA: 50 nM) were tested in MDA-MB-231-Luc cells and HepG2-Luc cells. Among all tests, the cells were treated with different formulations for 24 h or 48 h. Each bar represents the mean ± SE of three experiments.

View Article Online
DOI: 10.1039/C8TB02706D

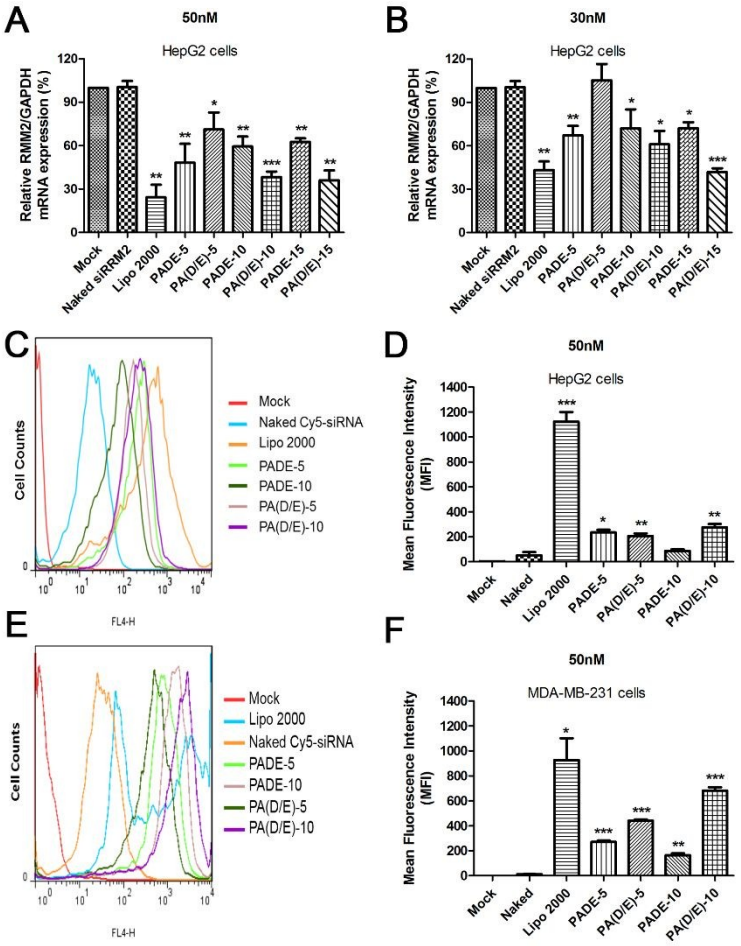

Fig. 6. RT-PCR assay was used to detect the RRM2 gene-silencing efficiencies of different vectors with the transfection concentrations of 50 nM (A) and 30 nM siRRM2 (B) respectively. The cell uptake detected by flow cytometry in histogram (C) and quantification(D) in HepG2 cell line. The cell uptake detected by flow cytometry in histogram (E) and quantification (F) in MDA-MB-231 cell line. The cell uptake was detected after HepG2 cells and MDA-MB-231 cells were transfected with PADE/siRNA and PA(D/E)/siRNA complexes for 4h, respectively. Each bar represents the mean ± SE of six experiments. *P < 0.05, **P < 0.01, and ***P < 0.001 vs naked Cy5-siRNA.

View Article Online
DOI: 10.1039/C8TB02706D

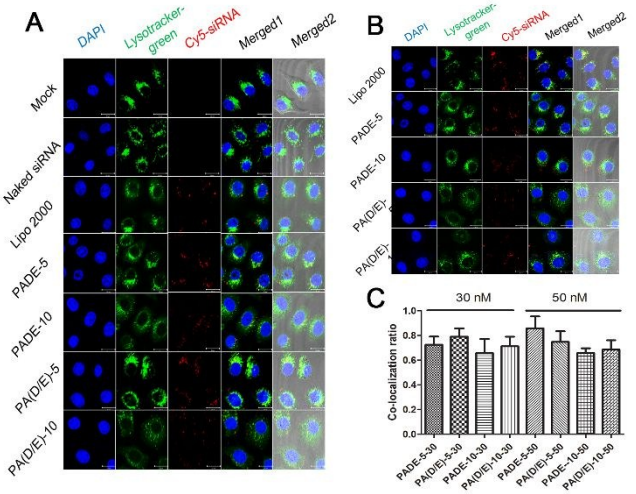

Fig. 7. Intracellular distribution of siRNA-loaded micelles in HepG2 cells at different N/P ratios with the transfection concentrations of siRNA were 30 nM (A) and 50 nM (B) determined by confocal laser scanning microscopy. (C) Statistics of colocated ratios of Cy5-siRNA and Lysotracker green. Each bar represents the mean ± SE of six experiments.

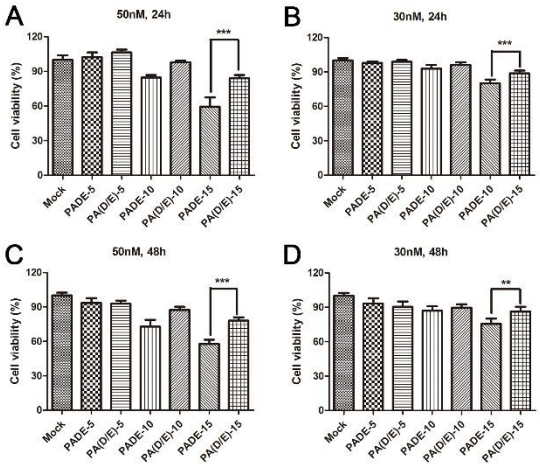

Fig. 8. In vitro cell viabilities of PADE and PA(D/E)/siRNA complexes at different N/P ratios with the transfection concentrations of siRNA were evaluated using MTT assay. In all tests, the HepG2 cells were treated with different formulations for 24 h or 48 h. siRNA dose: 30 nM and 50 nM. Each bar represents the mean ± SE of three experiments. *P < 0.05, **P < 0.01, and ***P < 0.001 vs naked PADE-15.